Article

Journal of
Nanoscience and Nanotechnology
Vol. 15, 1805–1814, 2015
www.aspbs.com/jnn

Localized Surface Plasmon Resonance in Au Nanoparticles Embedded dc Sputtered ZnO Thin Films

Anuradha Patra[1], M. Balasubrahmaniyam[1], Ranjit Laha[1], P. Malar[2], T. Osipowicz[2], A. Manivannan[3], and S. Kasiviswanathan[1,*]

[1] Department of Physics, Indian Institute of Technology, Madras, Chennai 600036, India
[2] Centre for Ion Beam Applications, National University of Singapore, Singapore 119260
[3] US Department of Energy, National Energy Technology Laboratory, Morgantown, WV 26507, US

The plasmonic behavior of metallic nanoparticles is explicitly dependent on their shape, size and the surrounding dielectric space. This study encompasses the influence of ZnO matrix, morphology of Au nanoparticles (AuNPs) and their organization on the optical behavior of ZnO/AuNPs–ZnO/ZnO/GP structures (GP: glass plate). These structures have been grown by a multiple-step physical process, which includes dc sputtering, thermal evaporation and thermal annealing. Different analytical techniques such as scanning electron microscopy, glancing angle X-ray diffraction, Rutherford backscattering spectrometry and optical absorption have been used to study the structures. *In-situ* rapid thermal treatment during dc sputtering of ZnO film has been found to induce subtle changes in the morphology of AuNPs, thereby altering the profile of the plasmon band in the absorption spectra. The results have been contrasted with a recent study on the spectral response of dc magnetron sputtered ZnO films embedded with AuNPs. Initial simulation results indicate that AuNPs–ZnO/Au/GP structure reflects/absorbs UV and infrared radiations, and therefore can serve as window coatings.

Keywords: Surface Plasmon Resonance, Optical Absorption, Gold Nanoparticles, ZnO Thin Films, Window Coatings.

1. INTRODUCTION

Metallic structures of sub-wavelength dimensions are characterized by a strong absorption band in the visible region of the electromagnetic spectrum. The extinction cross-section experiences a resonant enhancement due to the interaction between the light induced surface plasmons and the perturbing radiation, manifesting in the localized surface plasmons resonance (LSPR) phenomenon.[1,2] The attributes of LSPR such as, the resonance position, FWHM, absorption maximum and modes exhibit an explicit dependence on the metallic material, the shape and size of the nanostructure as well as on the dielectric constant of the surrounding medium. For instance, Au nanoparticles (AuNPs) in water exhibit LSPR at ~520 nm, whereas, Ag nanoparticles (AgNPs) in the same dielectric space show LSPR at ~420 nm.[3] Prolate metallic nanoparticles, on the other hand are typical examples of nanostructures that exhibit shape dependent LSPR. For instance, Au nanorods show two LSPR modes: Transverse and longitudinal modes. The former is located at ~520 nm while the resonant position of the latter, depending on the aspect ratio, falls in the spectral region from visible to near infrared. The material dependence as well as the matrix dependence of LSPR, under dipole approximation can be described by the resonance condition, $|\varepsilon_1 + 2\varepsilon_r| = 0$, where ε_1 and ε_r are the real parts of the dielectric function of the nanoparticle and the surrounding matrix respectively. For non-spherical nanoparticles, the resonance condition is slightly modified and is expressed as $\varepsilon_1 = -\chi\varepsilon_r$.[4] The parameter χ accounts for the shape of the nanoparticles and is a function of aspect ratio. This relation leads to morphology and space dependent LSPR characteristics. The freedom of manipulating the outcome of the interaction by any of the parameters

*Author to whom correspondence should be addressed.

discussed has been a guiding principle in the field of plasmonics.[3, 5]

By incorporating metal particles in transparent conducting oxide (TCO) matrix, the functional property of the former can be used to improve the functionality of the two-phase composite system. Xiao et al.[6] ion implanted ZnO films grown on SiO_2 substrates with Ag ions, leading to the formation of AgNPs in ZnO film. The authors found a large increase in the photoluminescence intensity in ZnO films embedded with AgNPs and attributed it to the resonant coupling between the surface plasmons of AgNPs and the spontaneous emission of ZnO. Recently, Yu et al.[7] reported bactericidal activity on AgNPs-TiO_2 composites formed using sol–gel technique. They observed that the composite films showed enhanced bactericidal activity compared to TiO_2 films, both under dark and UV illumination. Chen et al.[8] proposed a structure for light-emitting diodes, consisting of metal/polymer layer/GZO/AgNPs/GP structure (GP: glass plate GZO: gallium doped zinc oxide). The authors observed a substantial increase in the electroluminescence intensity due to the strong coupling of excitons with localized surface plasmons. The composite system consisting of AuNPs dispersed in ZnO matrices have shown large non-linear optical coefficients.[9, 10] Ryasnyanskiy et al.[9] have used rf sputtering of a composite target consisting of ZnO and Au wires to form ZnO films embedded with AuNPs and studied their nonlinear optical response. They found the real part of third-order nonlinear optical susceptibility to be -14.7×10^{-8} esu, at 532 nm. Ning et al.[10] reported nonlinear optical measurements on AuNPs–ZnO composite films formed on quartz substrate using nanosphere lithography. The real and imaginary parts of the third-order nonlinear susceptibility were reported to be 1.15×10^{-6} esu and -5.36×10^{-6} esu respectively, at 532 nm. Moreover, AuNPs embedded ZnO films were shown to have potential for optical filters.[11]

The present work is concerned with the optical behavior of multilayer structures in which AuNPs–ZnO composite is an integral part. Recently, we have reported the optical response of AuNPs embedded in dc magnetron sputtered ZnO films.[12] Here, we present the spectral response of AuNPs embedded in dc sputtered ZnO films. The microstructure and dielectric function of dc sputtered ZnO films were found to be different from that of dc magnetron sputtered ZnO films, and this served as a motivation to study the optical response of dc sputtered ZnO films embedded with AuNPs in detail. Interestingly, with increase in AuNPs size in dc sputtered ZnO films, the LSPR peak positions, absorption maxima and FWHM have exhibited different magnitude of variation. Hence, after each step of fabrication of the multilayer structure glancing angle X-ray diffraction (GXRD), scanning electron microscopy (SEM) and optical transmittance measurements have been made in order to understand the observations.

2. EXPERIMENTAL DETAILS

A multiple step process involving deposition of ZnO films and Au films, and thermal annealing was used to form ZnO films embedded with AuNPs. Initially, a thin ZnO film is deposited by dc sputtering on glass plate (GP) and is denoted as ZnO/GP. Sputtering was done at constant power mode (100 W) in the presence of argon (1%) and oxygen (99%) gas mixture. The target was 4 N pure circular Zn disc (3″ in diameter and 0.25″ in thickness). The base pressure achieved in the chamber was $\sim 2 \times 10^{-6}$ mbar. The chamber pressure during sputtering was 5×10^{-2} mbar. On ZnO/GP, a thin Au film of desired thickness is then deposited by thermal evaporation, resulting in Au/ZnO/GP structure. This was followed by annealing at 400 °C in flowing oxygen for 2 hours. During annealing, the Au film dewets and eventually agglomerates into randomly distributed AuNPs on the surface of ZnO film. This structure is denoted as AuNPs/ZnO/GP. Finally, a sufficiently thick ZnO film was sputtered over the AuNPs/ZnO/GP structure. The resultant structure was treated as AuNPs–ZnO composite film in between two ZnO films and is denoted as ZnO/AuNPs–ZnO/ZnO/GP structure. This configuration has been mainly used for all the analyses including Rutherford backscattering spectrometry (RBS).

The samples were characterized by different analytical techniques. Glancing angle X-ray diffraction (GXRD) measurements were carried out in a PANalytical (model: X'Pert PRO) XRD unit using Cu-Kα radiation. The glancing angle was optimized to collect maximum intensity and was kept fixed at 1.5° for all the samples. The reflections from GXRD pattern were indexed and compared with the JCPDS standards. Surface morphological studies were performed by scanning electron microscopy (SEM), and compositional homogeneity and interface properties were studied by RBS. SEM measurements were carried out on films grown on Si substrates using FEI (model: Quanta 200) scanning electron microscope. RBS measurements were carried out using the Singletron 3 MV accelerator facility at the Centre for Ion Beam Applications (CIBA), National University of Singapore, Singapore. Normally incident $^4He^{++}$ ions of energy 2 MeV and current ~ 5 nA were used as incident ion beam. The backscattered particles were collected at an angle of 170° using a surface barrier detector. Optical response of the films was studied using UV-VIS-NIR optical spectroscopy. Transmittance measurements at normal incidence were made using Jasco V-570 spectrophotometer in the wavelength range 200–2500 nm.

The optical constants of the films have been extracted from the transmittance spectra by adopting suitable dielectric function models, using a computer code.[13] For ZnO films (ZnO/GP), a composite dielectric function that combines the Drude model with O'Leary–Johnson–Lim, (OJL) model was considered. Drude model describes the optical

absorption in the near infrared region that is dominated by free carriers. The UV-VIS region of the transmittance spectrum is described by the OJL model that accounts for the band-to-band transition. The OJL model assumes parabolic conduction and valence bands, with exponentially decaying tail states. The optical response of the remaining structures (Au/ZnO/GP, AuNPs/ZnO/GP and ZnO/AuNPs–ZnO/ZnO/GP) involved stack-by-stack modeling. In all cases, the dielectric function of ZnO film has been described by a combination of OJL and Drude terms. It is important to note that all the three structures consist of a two-phase composite system. Since a thin film of Au is deposited over ZnO film, the Au film can be treated as Au-Air composite film, essentially a semi-continuous Au film. Thus, the Au/ZnO/GP structure is modeled with a layer stack of Au-Air composite on ZnO coated GP (Au-Air/ZnO/GP). Similarly, AuNPs/ZnO/GP structure is visualized as AuNPs-Air/ZnO/GP structure. The resulting structure formed after the deposition of ZnO film over AuNPs-Air/ZnO/GP structure, as described earlier has been modeled as AuNPs–ZnO composite sandwiched between ZnO films.

While the plasmonic properties of spherical nanostructures, can be described by Mie theory, an exact analytical solution cannot be obtained for nanostructures of lower symmetry such as cubes, triangles or spheroids. Various numerical methods have been developed to understand the plasmonic behavior of such nanostructures. Some of the notable examples include discrete dipole approximation (DDA), finite difference time domain (FDTD) and finite element method (FEM). All three numerical methods, depending upon the problem, can be used to get the near-field distribution of electric field as well as the scattering cross section. Since the aim here is to study the optical response of nanostructure in terms of the dielectric function of the composite media, effective medium theory has been used. Optical responses of Au-Air, AuNPs-Air and AuNPs–ZnO composite media can be described within the framework of classical effective medium theories because the extension of nanostructures is much smaller than the wavelength of incident radiation.[1] Therefore, the composites can be associated with an effective dielectric function, ε_{eff}, which governs the light propagation inside the two-phase (heterogeneous) system. Because of the randomness associated with the shape, size and inter-particle separation of AuNPs in the composite media, direct evaluation of optical constants using simple mixing formula consisting of average of dielectric function of constituents and volume fractions is difficult.

Optical response of two-phase composite systems has been analyzed using Bergman-Milton formulation[14] with the help of a computer code.[13] For Au, the dielectric function data available in the literature[15] is used. Bergman formulated an integral representation of effective dielectric function for two-phase disordered composite by solving some exact inequalities. In Bergman-Milton representation, ε_{eff} is expressed in terms of a positive spectral density function, $g(m)$, which is characteristic of the geometry and is given by,

$$\frac{\varepsilon_{\text{eff}}}{\varepsilon_r} = 1 - \int_0^1 \frac{g(m)}{s-m}\, dm \qquad (1)$$

where, the material constants enter through complex variable s, known as reduced dielectric function. The numerical analysis of the integral in Eq. (1) is facilitated by discretizing the integral under suitable conditions.[16] ε_{eff} can then be expressed in terms of ε_r, the dielectric constant of the matrix, volume fraction and a parameterized term which in turn can be written in the form of a continued fraction.[16] The continued fraction contains s and few parameters that are related to the moments of $g(m)$. The continued fractions can be used to construct the spectral density appearing in the Stieltjes integral (Eq. (1)) and henceforth, useful information in the context of shape, size and organization of the nanoparticles can be extracted, as has been discussed in Ref. [12], in addition to the extraction of ε_{eff}.

3. RESULTS AND DISCUSSION

Figures 1(a)–(d) summarize the variation in GXRD patterns obtained at different stages of growth of dc sputtered ZnO films embedded with AuNPs. The pattern for as-deposited ZnO film on glass plate (Fig. 1(a)) shows three peaks corresponding to reflections from (100), (002) and (101) planes of ZnO. Figure 1(b) shows the GXRD pattern for Au/ZnO/GP structure obtained after the deposition

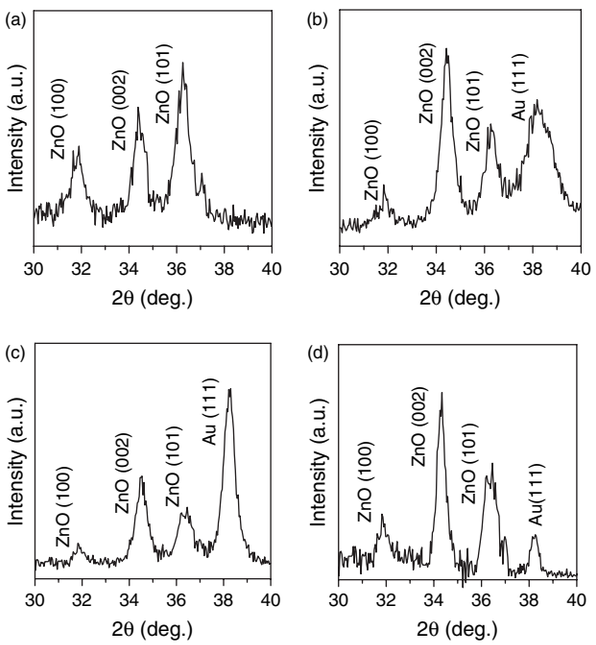

Figure 1. Evolution of GXRD pattern during different stages of formation of dc sputtered ZnO films embedded with AuNPs. (a) ZnO/GP, (b) Au/ZnO/GP, (c) AuNPs/ZnO/GP and (d) ZnO/AuNPs–ZnO/ZnO/GP structures.

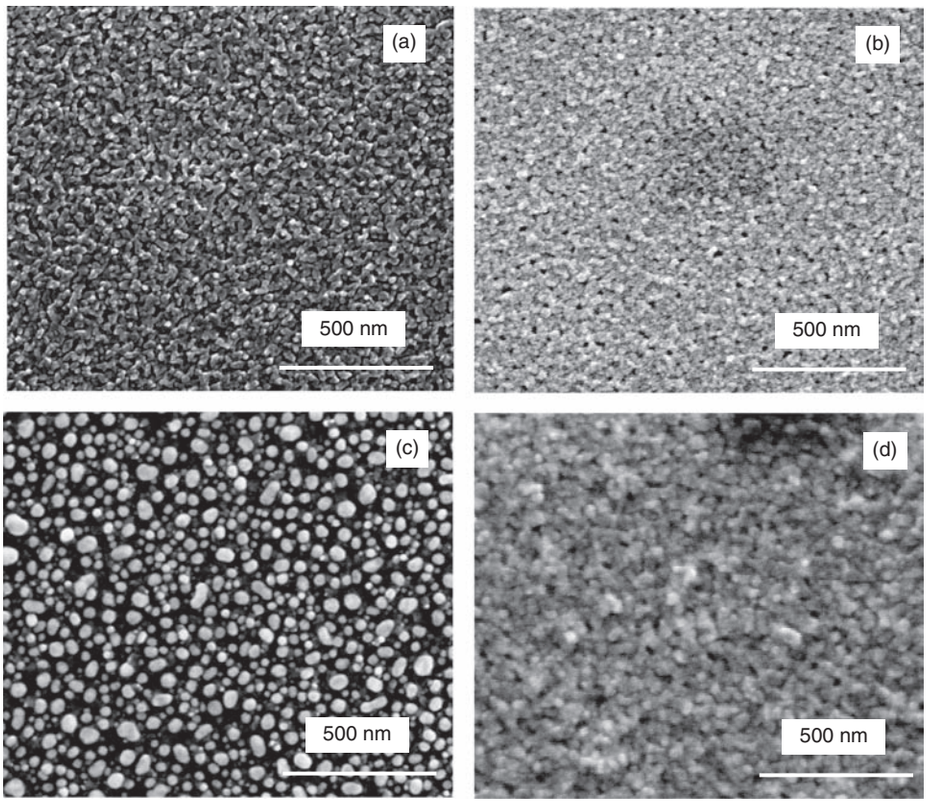

Figure 2. SEM images (a) ZnO/Si, (b) Au/ZnO/Si, (c) AuNPs/ZnO/Si and (d) ZnO/AuNPs–ZnO/ZnO/Si structures.

of ∼6 nm thick Au film over ZnO film. An additional peak appears at the 2θ value, 38.5° and is identified as Au (111) plane. Further, there is noticeable increase in the intensity of 002 ZnO peak. Figure 1(c) shows the pattern obtained after annealing the Au/ZnO/GP structure that is crucial to AuNPs formation. As seen from Figure 1(c), annealing has increased the Au 111 peak height, which is expected.[17] GXRD pattern obtained after depositing the top ZnO film (Fig. 1(d)) shows that there is significant increase in the intensity of ZnO peaks. This is because of the net increase in interaction volume for X-rays, as both the top and bottom ZnO films will contribute to the diffracted X-ray intensity.

SEM images taken after each stage of formation of dc sputtered ZnO film embedded with AuNPs are displayed in Figures 2(a)–(d). SEM image of the as deposited film is displayed in Figure 2(a). The micrograph shows grains without any specific shape, unlike the dc magnetron sputtered ZnO thin film that exhibited nanometer grains.[12] Formation of larger ZnO grains and different morphology in case of dc sputtered ZnO film is attributed to different growth conditions. In dc sputtering, the substrate is constantly bombarded by high energy secondary electrons and subsequently the substrate temperature reaches ∼450 °C.[18] Hence the ZnO grains may coalesce together and form larger grains. Figure 2(b) shows the SEM image taken after the deposition of ∼6 nm thick Au film. The morphology of the Au film is featureless, which after annealing turns into well-defined, but randomly distributed nanoparticles (Fig. 2(c)). The AuNPs are oriented predominantly along (111) direction as the corresponding GXRD pattern showed significant increase in the intensity of Au 111 peak. Further, as discussed earlier, the growth in the direction normal to the substrate may also enhance the diffracted X-ray intensity. Figure 2(d) represents the SEM image of the ZnO/AuNPs–ZnO/ZnO/Si structure, which is obtained after the deposition of a relatively thicker top ZnO film. The ZnO film completely covers the AuNPs. A close observation of Figure 2(d) reveals that certain areas on the surface have features that resemble the morphology of the as-deposited ZnO film (Fig. 2(a)).

Quantitative information regarding thickness and elemental composition of different layers can be derived from RBS.[19] The samples for RBS studies were grown on Si substrates with thermally grown SiO_2 (SiO_2/Si substrates). SiO_2/Si were chosen instead of Si so as to avoid interface formation during ZnO deposition. Any interface formed would increase the number of unknowns during analysis. The ZnO/AuNPs–ZnO/ZnO/SiO_2/Si structure was studied by RBS. Conventional procedure available for analyzing RBS spectrum, however, cannot be used for simulating the RBS spectrum of ZnO/AuNPs–ZnO/ZnO/SiO_2/Si structure since conventional method assumes homogeneous mixture of different elements at atomic level. When there is no

lateral homogeneity, i.e., when the sample consists of inhomogeneous mixture of two or more phases, the assumption of uniformity at atomic level in any plane parallel to the surface is no more applicable. Therefore, conventional simulation may not reproduce the RBS spectra satisfactorily and if it does, the results may be erroneous.[20]

The sample under study consists of an inhomogeneous mixture of AuNPs and ZnO, sandwiched between ZnO films. As the incident ion beam with diameter of ∼1 mm traverses the layer containing ZnO and AuNPs, some part of the beam may encounter the homogeneous ZnO film all through its path, until it meets the substrate. Some other part of the same beam may encounter Au (in the middle layer) before reaching the substrate. In such a situation, a simple method[21] based on weighted sum of two different homogenous structures can be used. The ZnO/AuNPs–ZnO/ZnO/SiO_2/Si structure is decomposed into two hypothetical structures with homogeneous individual layers: One with a thick ZnO film over SiO_2/Si substrate and the other with a thin Au film sandwiched between ZnO thin films. Thus, the RBS spectra of ZnO/SiO_2/Si and ZnO/Au/ZnO/SiO_2/Si structures were first generated independently (with conventional simulation method) and the net yield was then calculated as a weighted sum of these two individual yields as,

$$Y_{\text{net}} = xY_{\text{ZnO/SiO}_2\text{/Si}} + (1-x)Y_{\text{ZnO/Au/ZnO/SiO}_2\text{/Si}} \quad (2)$$

Apart from the thickness and composition of the elements in the individual layers, the weight (x) was also varied. In addition, the option "fuzzing" was used to account for the layer roughness.

RBS spectrum of dc sputtered ZnO film embedded with AuNPs, formed with initial effective Au film thickness of ∼5 nm is displayed in Figure 3. The open circles denote the experimental data, while the continuous line through the data points denotes the simulated data. The distinct single peak that appears just beyond 1.6 MeV is due to Au. The yield due to Zn appears as a broad peak with a dip nearly in the middle. The front edge of the Zn peak is due to the Zn atoms on the surface of the top ZnO film, while the back edge is due to Zn atoms present at the boundary between ZnO film and SiO_2. The dip is due to the AuNPs–ZnO layer in which the concentration of Zn is low, compared to the other regions of the ZnO film. There are two Si edges, which are marked by arrows in Figure 3. The edge appearing at higher energy value is due to Si atoms from SiO_2 film and the other is due to the Si atoms from the Si substrate. The yield due to oxygen appears as a superimposed broad peak on the Si plateau. It has contributions from oxygen atoms from both ZnO and SiO_2. The simulations yield a value of 0.83 for the weight parameter (x). Although, the weighted sum method reproduces the experimental data well, further refinements are necessary for exact calculation. Moreover, due to the assumption of a thin continuous Au film (with

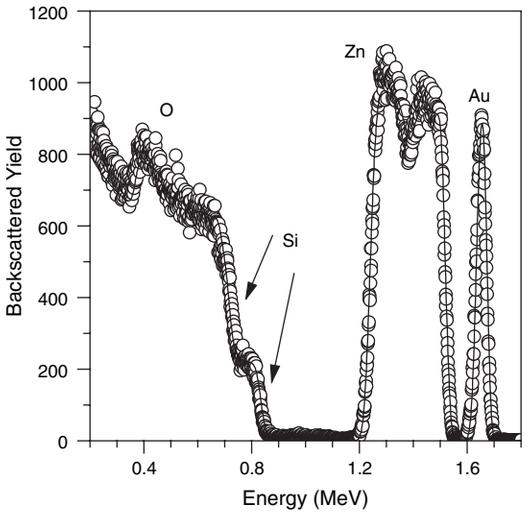

Figure 3. Typical RBS spectra of ZnO/AuNPs–ZnO/ZnO/SiO_2/Si structure. Open circles denote the experimental data and the continuous line through the data points represents the XRUMP simulation by weighted sum method.

the boundaries/interface being sharp), the vertical height of AuNPs may be underestimated. Nevertheless, the RBS simulation of ZnO/AuNPs–ZnO/ZnO/SiO_2/Si structure by weighted sum method does help in providing elemental composition of the film and gives confirmation, in accordance with GXRD and SEM studies, that annealing of thin Au film leads to the formation of AuNPs. For instance, the thickness of Au film obtained from the simulation was ∼32 nm, which is larger than the effective thickness of the initial Au film (∼5 nm) in Au/ZnO/SiO_2/Si structure by a factor of 6, casting evidence that annealing has led to huge increase in the out-of-plane height of Au. The result, as will be seen in the following paragraphs, also corroborates the optical analysis.

The results obtained from the numerical fit to the optical transmittance spectra recorded after each stage of fabrication of dc sputtered ZnO film embedded with AuNPs are displayed in Figure 4. The open symbols and the continuous lines denote the experimental data and the fit to the data respectively. The average transmittance of ZnO/GP structure is more than 80% in the visible and near infrared regions, and the characteristics are similar to the dc magnetron sputtered films.[12] The transmittance of Au/ZnO/GP structure (open squares, Fig. 4(a)) falls considerably in the near infrared region and shows a dip at ∼750 nm. This indicates the formation of discontinuous Au film which is considered as Au-Air composite film for the purpose of analysis. The corresponding spectral density function (dark line, Fig. 4(b)) shows a peak close to origin and it suggests that the Au film structure is close to forming percolative network.

The distinct minimum in the transmittance spectrum (open diamonds, Fig. 4) of AuNPs-Air/ZnO/GP structure at ∼564 nm reflects the formation of AuNPs and it

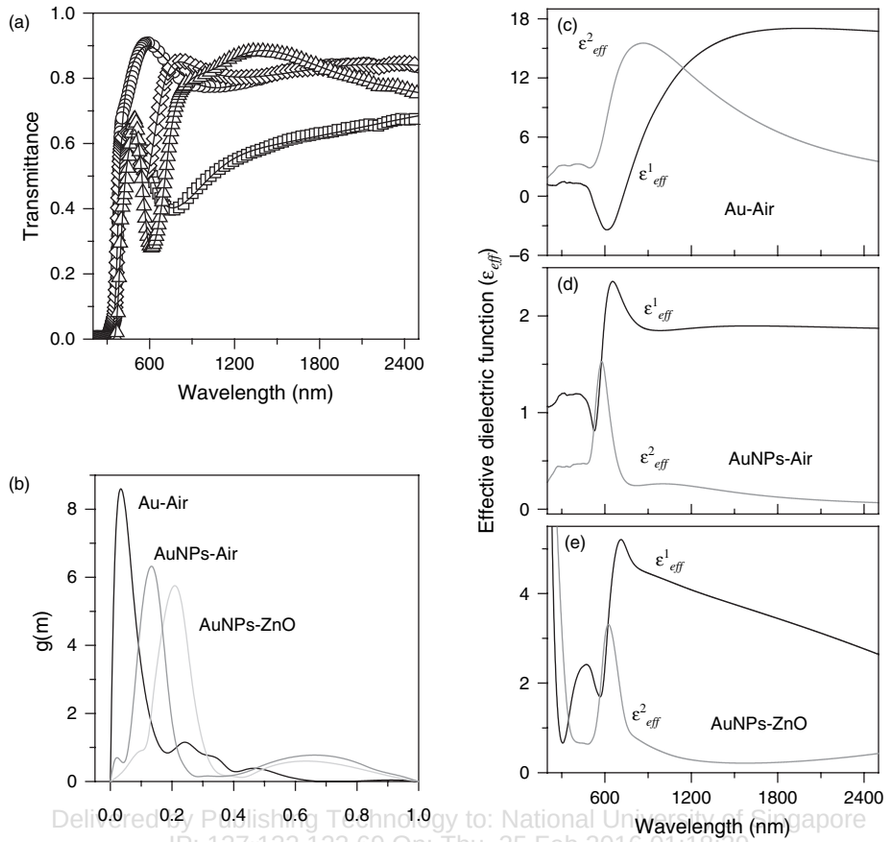

Figure 4. (a) Transmittance spectrum of (◯) ZnO/GP, (□) Au/ZnO/GP, (◊) AuNPs/ZnO/GP and (△) ZnO/AuNPs–ZnO/ZnO/GP structures. The continuous line through the data points denote fits to the data. (b) Spectral density function of Au-Air (dark line), AuNPs-Air (dark grey lines) and AuNPs–ZnO (light grey line) composite films. (c)–(e) Effective dielectric function of composite films. $\varepsilon^1_{\text{eff}}$ and $\varepsilon^2_{\text{eff}}$ are denoted by dark and grey lines respectively.

manifests as shift of the peak in $g(m)$ (dark grey line, Fig. 4(b)) towards higher m. The shift of LSPR minimum to ∼610 nm (open triangles, Fig. 4(a)) brought by the addition of top ZnO film is seen as a right-shift of peak in $g(m)$, apart from reduction of its strength (light grey, line Fig. 4(b)). Further, as seen from Figures 4(c)–(e), $\varepsilon^1_{\text{eff}}$ shows anomalous dispersion while $\varepsilon^2_{\text{eff}}$ shows absorption corresponding to LSPR wavelength. The relevant parameters obtained from the fit are summarized in Table I. It is to be noted here that the thickness of Au-Air composite and the volume fraction of Au (step 2) were 10.4 nm and 61% respectively which changed significantly after Au/ZnO/GP was annealed. The thickness of AuNPs-Air composite increased to 55.3 nm whereas the volume fraction of Au reduced to 12%. Upon addition of the top ZnO film (step 4), the AuNPs-Air composite changes to AuNPs–ZnO composite with 62.5 nm in thickness (an increase by a factor of 6, w.r.t the initial Au film thickness) and the volume fraction of Au decreases further from 12 to 9%. These observations can be understood based on mass conservation of Au. For a given surface area of the substrate and mass of Au, when the thin Au film agglomerates to form AuNPs (step 3), redistribution of Au takes place in the form of growth along the vertical direction. This process must occur at the expense of surface area coverage, essentially leading to increase in the space available

Table I. Parameters obtained from the fit to transmittance spectra.

Fabrication step	Structure considered for analysis	Thickness (nm)			Au volume fraction (V_f)
		Bottom ZnO film	Composite film	Top ZnO film	
Step 1 deposition of ZnO film	ZnO/GP	207	–	–	–
Step 2 deposition of Au film	Au-Air/ZnO/GP	207	10.4 (Au-Air)	–	0.61
Step 3 annealing at 400 °C	AuNPs-Air/ZnO/GP	207	55.3 (AuNPs-Air)	–	0.12
Step 4 deposition of top ZnO film	ZnO/AuNPs–ZnO/ZnO/GP	207	62.5 (AuNPs–ZnO)	164	0.09

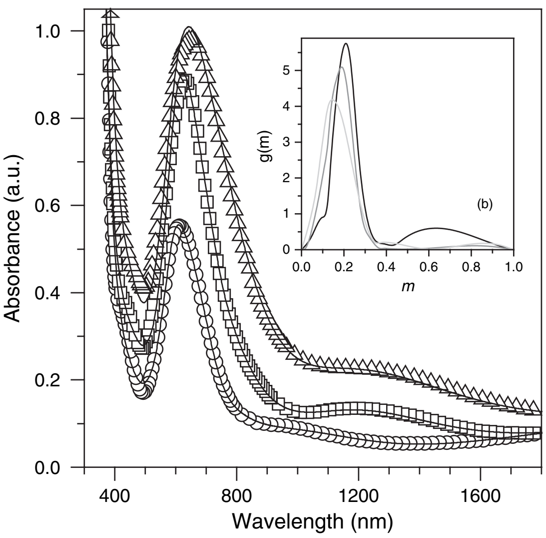

Figure 5. Absorbance spectrum of ZnO/AuNPs–ZnO/ZnO/GP structure for Au film thickness of 6 nm (triangles) 10 nm (squares) and 15 nm (circles). The continuous lines through the symbols denote the fits. (Inset) Spectral density functions for the AuNPs–ZnO composite film formed with initial Au thickness of 6 nm (dark line), 10 nm (dark grey line) and 15 nm (light grey line).

in between AuNPs. The changes in step 4 indicate that, during dc sputtering the AuNPs undergo additional physical changes. The principal reason is the bombardment of AuNPs by secondary electrons and other high-energy species, and the consequent increase in substrate temperature to ∼450 °C during the deposition of top ZnO film.[18] Hence, the AuNPs undergo additional thermal treatment during sputter deposition of ZnO film. It may be noted here that the maximum temperature to which the initial Au films are taken to induce agglomeration and formation of AuNPs is ∼400 °C which is less than the temperature reached when the ZnO films are grown.

In order to study the effect of initial Au film thickness, ZnO/AuNPs–ZnO/ZnO/GP structures were fabricated with Au films of three different initial thicknesses. Figure 5 shows the absorbance spectra of ZnO/AuNPs–ZnO/ZnO/GP structures with Au films of mass thickness ∼6 nm (open circles), ∼10 nm (open squares) and ∼15 nm (open triangles). The continuous lines drawn through the data points in Figure 5 denote the theoretical fit. As the film thickness increases, the LSPR maximum shows red-shift in wavelength and appears at 610, 634 and 650 nm for structures fabricated with 6, 10 and 15 nm thick Au films respectively. The corresponding spectral density functions are displayed in inset to Figure 5. Displacement of absorbance maxima towards higher wavelength and a corresponding systematic shift in $g(m)$ peak towards lower m values accompanied by decrease in peak height is the signature of the presence of larger AuNPs in AuNPs–ZnO composite films.[12] The physical significance lies in the fact that increase in initial Au film thickness leads to the formation of larger AuNPs (AuNPs of lower symmetric shape) with lesser number density. The interference of higher order modes is induced then and the LSPR peak shifts to longer wavelengths as a result.[1]

With a view to probe the effect of number density of particles on LSPR profile, ZnO/AuNPs–ZnO/ZnO/AuNPs–ZnO/ZnO/GP structure, a "two-stack" structure having two AuNPs–ZnO composite films has been studied. Figure 6(a) shows the transmittance spectrum of two-stack and ZnO/AuNPs–ZnO/ZnO/GP structures together with the fits (dark lines through the symbols). In Figure 6(a), the open circles denote the spectrum of two-stack structure, while the open squares denote that of ZnO/AuNPs–ZnO/ZnO/GP structure. The latter spectrum was included for the sake of comparison. The thickness of the Au films used to form both AuNPs–ZnO layers was kept same and was ∼10 nm. The two-stack structure shows an increase in the transmittance minimum. There is no noticeable shift in the LSPR position, but the LSPR peak is quite broad and extends to about 1200 nm. The increase in absorption strength without shift in the peak position indicates that there is definite and significant increase in the number density of particles. The broadening may be due to the increase in the number density of particles having larger average size. Further insight into LSPR profile can be gained from the SEM image (Fig. 6(b)) obtained after annealing the second Au film, i.e., the image of AuNPs/ZnO/AuNPs–ZnO/ZnO/Si structure. The surface morphology resembles that of AuNPs/ZnO/Si structures, which is displayed in Figure 2(c). But, there is noticeable increase in the particle size, which confirms the conclusions drawn based on the LSPR minimum in the transmittance spectrum (Fig. 6(a)). Since the thickness of the ZnO-spacer film is sufficiently large (pl. see Fig. 2(d) for the SEM image of the surface of spacer film) this structure is assumed to have the layer sequence viz., ZnO/AuNPs–ZnO/ZnO/AuNPs–ZnO/ZnO/GP, for the purpose of numerical fit. However, attempts to model with two AuNPs–ZnO composites having identical characteristics were unsuccessful. A satisfactory fit to the experimental data required the two AuNPs–ZnO composite be treated as independent layers with different spectral density functions. In other words fit was possible, only when the microstructure of the two AuNPs–ZnO media were assumed to be different, in spite of the fact that Au films used were of same thickness (10 nm). Thus, the structure considered can be written as ZnO/$(\text{AuNPs–ZnO})_2$/ZnO/$(\text{AuNPs–ZnO})_1$/ZnO/GP, where the subscripts denote the order (position) of the two composite media, which have same constituents with different microstructure and volume fraction. Inset to Figure 6(a) shows the spectral density functions of the two AuNPs–ZnO composite films. In Figure 6(a), $g_1(m)$ and $g_2(m)$ denote the spectral density function of the bottom, viz., $(\text{AuNPs–ZnO})_1$ and the top viz., $(\text{AuNPs–ZnO})_2$ composite films respectively. The spectral density functions differ significantly and the

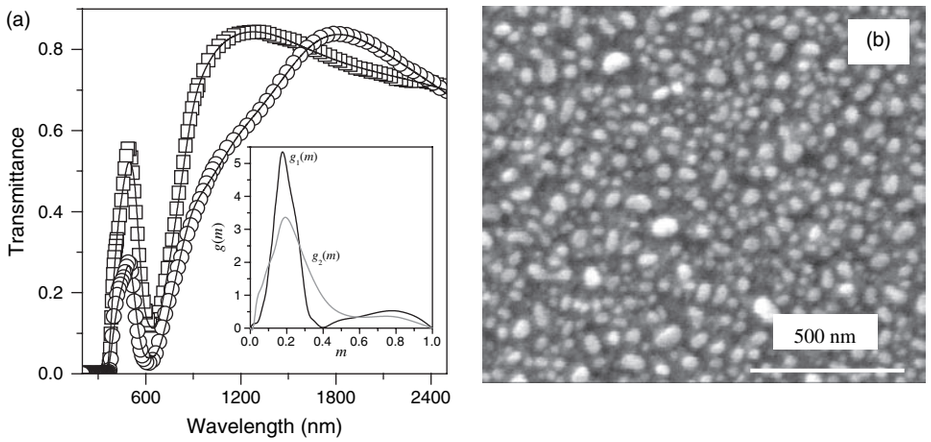

Figure 6. (a) Transmittance spectrum of (□) ZnO/AuNPs–ZnO/ZnO/GP structure and (○) ZnO/AuNPs–ZnO/ZnO/AuNPs–ZnO/ZnO/GP structure. The dark lines through the symbols denote fits. (Inset) Spectral density function of the bottom (dark line) and the top (grey line) AuNPs–ZnO composite films in ZnO/AuNPs–ZnO/ZnO/AuNPs–ZnO/ZnO/GP structure. (b) SEM image of AuNPs formed over ZnO/AuNPs–ZnO/ZnO/Si structure, the SEM image of which is displayed in Figure 4.21(d). The Au film thickness is ∼6 nm.

difference may arise due to the difference in size/shape and physical arrangement of AuNPs in $(AuNPs–ZnO)_1$ and $(AuNPs–ZnO)_2$ composite films. A possible reason may be that the surfaces offered to the growth of Au film and hence to the formation of AuNPs are not identical.

It is interesting to compare the optical characteristics of ZnO/AuNPs–ZnO/ZnO/GP structures fabricated with dc sputtered ZnO films and dc magnetron sputtered ZnO films reported in Ref. [12]. Although the trends observed in the optical characteristics are mostly similar, certain important differences are noticed. First, the LSPR minimum observed for AuNPs embedded in dc sputtered ZnO films are symmetric and they remained so (Fig. 5), even when thickness of the initial Au film was 15 nm, which is the maximum thickness used. However, the LSPR peaks in structures with dc magnetron sputtered ZnO films were asymmetric and the asymmetry increased with thickness of the initial Au film.[12] The other differences are presented in Figures 7(a)–(c), which summarize the variations of LSPR maximum (λ_{max}), absorbance value (A_{max}) corresponding to λ_{max} and FWHM of the LSPR peak, respectively with respect to initial Au film thicknesses. The open and filled symbols correspond to ZnO/AuNPs–ZnO/ZnO/GP structures for dc magnetron sputtered ZnO and dc sputtered ZnO films respectively. The dashed and dotted lines through the symbols are to guide the eye. As seem from Figure 7(c), varying the initial Au thickness from 6 nm to 15 nm the λ_{max} varied from 610 nm to 650 nm only for structures formed with dc sputtered ZnO (filled circles), whereas in the case of structures formed with dc magnetron sputtered ZnO films a variation of 5 nm to 10 nm in initial Au film thickness produced a shift in λ_{max} from 612 nm to 684 nm (open circles). The absorbance value (A_{max}) corresponding to λ_{max} is higher for samples formed with dc sputtered ZnO (filled square, Fig. 7(b)) in comparison to those with dc magnetron sputtered ZnO (open square, Fig. 7(b)). The variation in FWHM is significantly higher for dc magnetron sputtered ZnO films embedded with AuNPs (open triangles, Fig. 7(a)) indicating higher losses in the films. The sensitivity of LSPR shift and

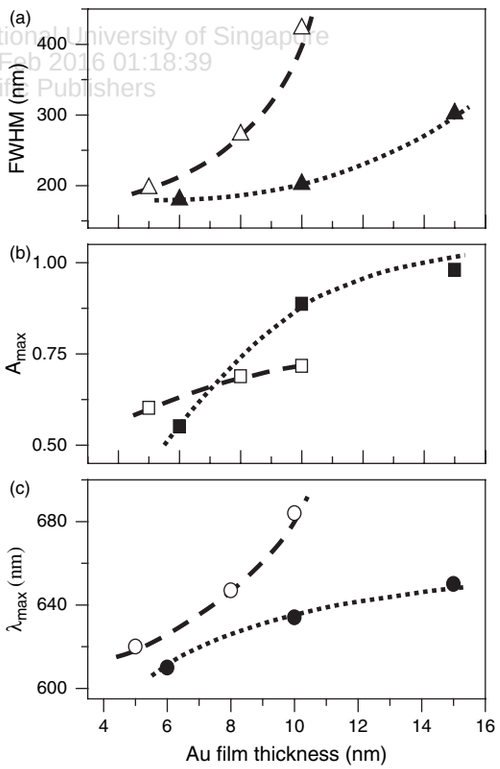

Figure 7. Variation of LSPR maximum (λ_{max}), absorbance value corresponding to λ_{max} (A_{max}) and FWHM of the LSPR peak for structures formed with dc magnetron (open symbols) and dc sputtered (filled symbols) ZnO films. The dashed and dotted lines through the data points are to guide the eye.

pronounced FWHM indicate that the AuNPs embedded in dc magnetron sputtered ZnO films are of lower symmetry than those embedded in dc sputtered ZnO films. For asymmetric nanoparticles, surface plasmons are unevenly distributed which, in turn gives rise to modes other than that due to dipole. Intervention of higher order modes decreases the dipole resonance strength and frequency, and leads to dynamical broadening of LSPR profile.

It is an established fact that LSPR position of asymmetric nanostructure exhibits greater sensitivity than that of symmetric nanostructure of comparable size.[4, 22, 23] In the work of Mock et al. the effect of AgNPs shapes viz., sphere, triangles and cubes, on LSPR properties was demonstrated.[22] It was found that the sensitivity ($=d\lambda_p/dn$, λ_p being the LSPR wavelength) of Ag nanotriangles (350 nm/RIU) was more than Ag nanospheres (160 nm/RIU). As another example to the particle shape effect on LSPR properties, Sun and Xia[23] showed that Au nanospheres and Au nanoshells of the same/comparable diameter exhibit different refractive index sensitivity. Au nanoshell typically exhibited sensitivity of 409 nm/RIU whereas, nanospheres of comparable diameter showed sensitivity of only 60 nm/RIU. Farland et al.[4] also documented that as the symmetry of nanostructure is reduced from sphere to rod-like, the refractive index sensitivity is increased.[4] In other words, it is also equivalent to say that in a fixed dielectric background, as the nanostructure size is increased, the extent of LSPR shift (sensitivity) will be more for elongated or distorted or oblate shaped particles than near spherical shaped nanostructures.

The primary reason behind formation of AuNPs with less asymmetry in dc sputtered ZnO film is the additional rapid heat treatment which the AuNPs (in AuNPs/ZnO/GP structure) receive during the top ZnO film deposition (Table I). Prior to top ZnO deposition, as in the case of AuNPs in dc magnetron sputtered films, an asymmetric AuNPs had formed by agglomeration (Fig. 2(c)). Rapid heat treatment during top ZnO film deposition, as discussed earlier, leads to a net increase in the average size of the AuNPs along the vertical (normal to substrate) direction and, in accordance with mass conservation, a net decrease in the average width (Table I). Therefore, the *in-situ* heat treatment may leads to reshaping of larger hemispherical AuNPs into near-spherical nanoparticles. AuNPs sandwiched in dc magnetron sputtered ZnO films, however, retain oblate shapes due to the absence of any such *in-situ* rapid heat treatment.[12]

It is of relevance to discuss the applications of the composite films consisting of ZnO films embedded with AuNPs. As an example, window coatings based on these composite films are considered theoretically. The typical structure chosen for window coating applications is AuNPs–ZnO/Au/GP. The effective dielectric function data used was that obtained for the AuNPs–ZnO formed with 6 nm thick Au film, and is shown in inset B in Figure 4. The thicknesses of the composite and the Au films are 100 nm and 30 nm respectively. These thicknesses were chosen so that there is finite transmittance in the visible region. Figure 8(a) shows the transmittance spectra of AuNPs–ZnO/Au/GP structure taken with AuNPs–ZnO composite film facing the incident beam. In Figure 8(a), the simulated transmittance, reflectance and absorptance spectra are denoted by dark line, grey line and light grey line respectively. It is important to note that reflectance increases sharply below 400 nm and is ~40% at 200 nm. Further, the transmittance is negligibly small below ~300 nm while the absorptance is significant. This indicates that the coating reflects about 50% of the UV radiations while the rest is absorbed. Similarly, beyond 1200 nm more than 80% of the incident radiation is reflected back. In other words, the structure does not allow the harmful UV radiation to pass through and also reflects back the unwanted infrared radiation. On the other hand, when the incident radiation falls on the glass side

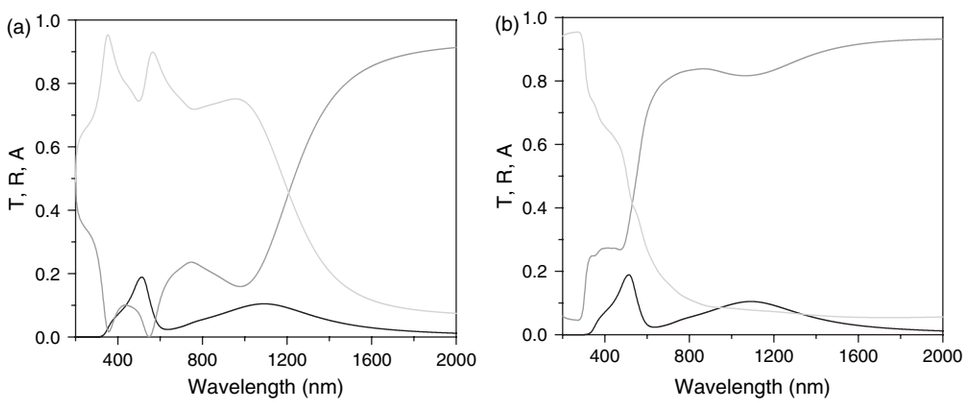

Figure 8. Characteristics of AuNPs–ZnO/Au/GP structures simulated assuming (a) the AuNPs–ZnO composite film to face the incident radiation and (b) the glass plate to face the incident radiation. In both figures, the dark line, grey line and the light grey line denote the transmittance, reflectance and absorptance respectively.

(Fig. 8(b)), about 70% of the radiation above 500 nm is reflected back. These are typical characteristics expected of window coatings used in hot climates. In addition, the coating, as mentioned earlier rejects UV radiation.

4. CONCLUSIONS

Evolution of the surface microstructure during different stages of ZnO/AuNPs–ZnO/ZnO/GP fabrication was investigated by combined GXRD, SEM, and optical absorption measurements. The AuNPs–ZnO composite medium consisting of randomly distributed AuNPs in ZnO matrix, in fact, evolved from an inverse geometry. A percolative-type Au-free space composite was first formed, which on annealing and subsequent ZnO deposition yielded AuNPs–ZnO composite. A semi-empirical approach based on Bergman's spectral density formulation was used to analyze the transmittance spectra and to extract the effective dielectric function of two-phase composite films. The results obtained were contrasted with the results of similar structures formed with dc magnetron sputtered ZnO films. Although the trends observed in optical absorption are similar for both films, certain important differences were noted and further analyses of the same lead to a definite conclusion that AuNPs embedded in dc sputtered ZnO films are of different geometry than that of AuNPs embedded in dc magnetron sputtered ZnO, although both have been grown with same initial Au film thickness and subjected to identical annealing treatment for agglomeration. It was recognized that in addition to the thickness of initial Au film, the *in-situ* rapid heat treatment during dc sputtering of ZnO films lead to significant alteration in the shape, size and distribution of AuNPs, which in turn cast subtle changes in the LSPR profile. For dc sputtered ZnO films embedded with AuNPs, spectral signature from near-spherical shaped AuNPs is observed, at variance with what was observed for dc magnetron sputtered ZnO films embedded with AuNPs. The embedded films can be grown over large area with relative ease and interestingly, initial results obtained from numerical simulations show that AuNPs–ZnO/Au/GP structure can serve as window coats with reasonable characteristics.

References and Notes

1. U. Kreibig and M. Vollmer, Optical Properties of Metal Clusters, Springer, Berlin (**1995**).
2. C. F. Bohren and D. R. Huffman, Absorption and Scattering of Light by Small Particles, Wiley, New York (**1983**).
3. M. Rycenga, C. M. Cobley, J. Zeng, W. Li, C. H. Moran, Q. Zhang, D. Qin, and Y. Xia, *Chem. Rev.* 111, 3669 (**2011**).
4. A. D. Farland and R. P. Van Duyne, *Nano Lett.* 3, 1057 (**2003**).
5. K. M. Mayer and J. H. Hafner, *Chem. Rev.* 111, 3828 (**2011**).
6. X. H. Xiao, F. Ren, X. D. Zhou, T. C. Peng, W. Wu, X. N. Peng, X. F. Yu, and C. Z. Jiang, *Appl. Phys. Lett.* 97, 071909 (**2010**).
7. B. Yu, K. M. Leung, Q. Guo, W. M. Lau, and J. Yang, *Nanotechnology* 22, 115603 (**2011**).
8. S.-H. Chen and J.-Yu. Jhong, *Optics Express* 19, 16843 (**2011**).
9. A. I. Ryasnyanskiy, B. Palpant, S. Debrus, U. Pal, and A. L. Stepanov, *Optics Communications* 273, 538 (**2007**).
10. T. Ning, Y. Zhou, H. Shen, H. Lu, Z. Sun, L. Cao, D. Guan, D. Zhang, and G. Yana, *Appl. Surf. Sci.* 254, 1900 (**2008**).
11. P. Anuradha and S. Kasiviswanathan, *International Journal of Nanoscience* 10, 601 (**2011**).
12. P. Anuradha, A. Manivannan, and S. Kasiviswanathan, *J. Opt. Soc. Am. B* 29, 3317 (**2012**).
13. W. Theiß, *Surf. Sci. Rep.* 29, 91 (**1997**).
14. D. J. Bergman, *Phys. Rep.* 43, 377 (**1978**); G. W. Milton, *J. Appl. Phys.* 52, 5286 (**1981**).
15. P. B. Johnson and R. W. Christy, *Phys. Rev. B* 6, 4370 (**1972**).
16. E. Gorges, P. Grosse, J. Sturm, and W. Theiß, *Z. Phys. B* 94, 223 (**1994**).
17. T. Shimizu, T. Teranishi, S. Hasegawa, and M. Miyake, *J. Phys. Chem. B* 107, 2719 (**2003**).
18. P. Malar, B. C. Mohanty, and S. Kasiviswanathan, *Thin Solid Films* 488, 26 (**2005**).
19. W. K. Chu, J. W. Mayer, and M. A Nicolet, Backscattering Spectrometry, Academic Press Inc., London (**1978**).
20. J. Schmitt, G. Decher, W. J. Dressick, S. L. Brandow, R. E. Geer, R. Shashidhar, and J. M. Calvert, *Adv. Mater.* 9, 61 (**1997**).
21. D. Mangelinck, P. S. Lee, T. Osipowitcz, and K. L. Pey, *Nucl. Instr. Meth. B* 215, 495 (**2004**).
22. J. J. Mock, M. Barbic, D. R. Smith, D. A. Schultz, and S. Schultz, *J. Chem. Phys.* 116, 6755 (**2002**).
23. Y. Sun and Y. Xia, *Anal. Chem.* 74, 5297 (**2002**).

Received: 9 June 2013. Accepted: 8 October 2013.